An essay on slope distributions and visibility

Hugh H. Kieffer File=-/krc/Doc/DV3/slopes.tex 2016oct

February 25, 2017

Contents

List of Figures

Abstract

Rough slopes and their effect on photometry and temperatures have been largely studied from a statisical approach, yielding results from modest to great mathmatical complexity; pragmatic simplifications are often involved. Yet, results that might represent a range of geologic morphologies are difficult to find. The goal here is to develop relatively simple mathmatical representations of slope distributions and "hiding" and visibiliity that can span [most] of the range of surfaces likely to be encountered on asteriods and that could be applied to thermal models without the invocation of radiosity.

The symbols <≫ and ≪> are used here to bound direct quotes from articles. Ellipsis, "..." indicate omitted material.

"p nnnn.f a" indicates the beginning location of a quote where nnnn is the page number, f is the decimal fraction of the way down the page, and a/b indicates the left/right column if on a two-column page.

Equation numbers mildly right of an equation are from the cited work; equation numbers at the right margin are sequential in this work.

1 History

Be alert that the rough-surface shadow function S commonly mentioned in the literature and here is the probability of NOT being in shadow.

1.0.1 Gaussian Distribution

Gaussian distribution: mean μ and stdDev σ

$$G_{(\sigma,\mu)} = \frac{1}{\sigma\sqrt{2\pi}} e^{-\frac{(x-\mu)^2}{2\sigma^2}}$$

Considering the solid angle at each slope, using a mean of zero, weighting by $\sin\theta$ so $\overline{\theta} = \int_{x=0}^{\pi/2} \frac{1}{\sigma\sqrt{2\pi}} e^{-\frac{x^2}{2\sigma^2}} \sin x dx$?? where did this come from ??

1.1 Smith 1967

Derives analytically the shadowing probability for a surface having a Gaussian distribution of elevations. [these old (slow computer era) guys were good at math!] His results are used by Bandfield, Davidsson and others? .

p 4059.8a <≫ The density of surface height deviations (ξ) from the mean plane in the z direction is described by a continuous probability function $P_1(\xi)$, of zero mean, chosen to be Gaussian for computational ease, where the probability of finding a height deviation within the range $\Delta\xi$ about ξ is

$$P_1(\xi)\Delta\xi = \frac{1}{(2\pi)^{1/2}\sigma} e^{-\xi^2/2\sigma^2} \cdot \Delta\xi \qquad (1)$$

where σ is the root-mean-square height deviation. ≪>

p 4060.1a <≫ The problem is the following: what is the probability $S(\xi_0, p_0, q_0, \theta)$ that a point F on a random rough surface, of given height ξ_0 above the mean plane and with local slopes p_0, q_0 will not lie in shadow when the surface is illuminated with a parallel beam of radiation at an angle of incidence θ to the mean plane? ≪>

$$2\Lambda(\mu) = \left(\left(\frac{2}{\pi}\right)^{1/2} \cdot \frac{w}{\mu} e^{-\mu^2/2w^2} - \text{erfc}\left(\mu/\sqrt{2}w\right) \right) \qquad (21)$$

p 4059.7, after Eq. 3: <≫ where w^2, [is] the mean square surface slope ≪>

p 4060.5b, after Eq. 9: <≫ where h is the unit step function and $\mu = \cot\theta$ ≪>

$$S(\theta) = \frac{\left[1 - \frac{1}{2}\text{erfc}\left(\mu/\sqrt{2}w\right)\right]}{[\Lambda(\mu) + 1]} \qquad (24)$$

p 4062.7a: <<>> ... the probability that a point on the surface with local slopes p, q will be illuminated by a beam of incidence angle θ is

$$S(p, q, \theta) = \frac{h(\mu - q)}{[\Lambda(\mu) + 1]} = S(q, \theta) \qquad (25)$$

(independent of p) where the subscripts have been dropped from p and q. <<>>

The basic function $S(\theta)$ of Smith67=[8] is shown in Fig. 1

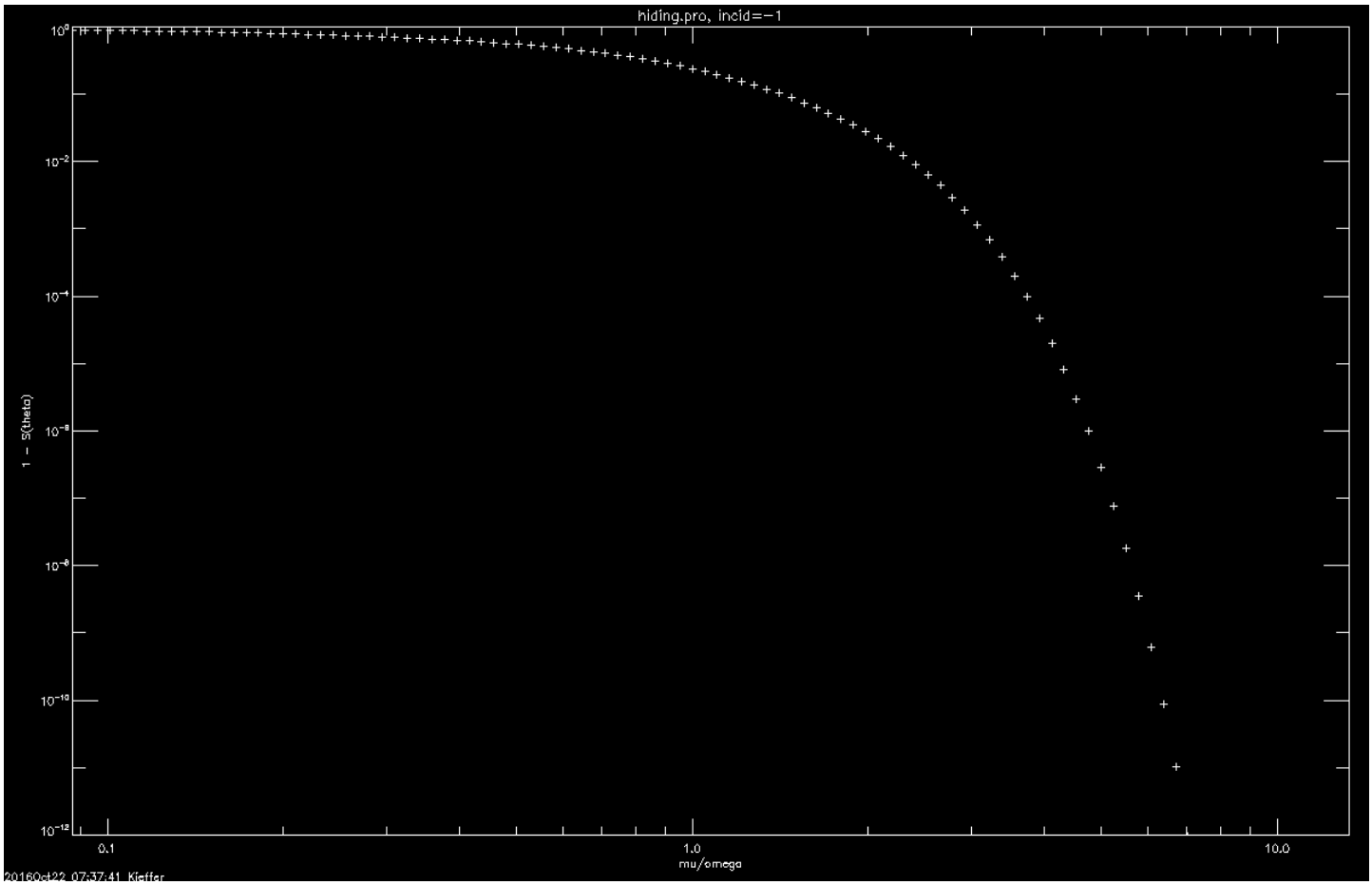

Figure 1: The basic shadow relation of Smith67=[8] as a function of $x \equiv \mu/w$ or cotangent of the incidence angle divided by the RMS roughness angle, plotted as logrithm of 1-$S(\theta)$, For small values of x S asymptotically approaches 0 and $S \to 1$ at large values of x. S difference from 1 is beyond the limit of single precision for $x > 5$. hids.png

The terms with $S(\theta)$ are shown in Fig. 2

In beaming.pro @48 I reproduce Fig. 2 of Smith67=[8] by calling **hiding.pro** with parameter[2]=-3, shown in Fig. 3

I should extract his results for both illumination and viewing shadows, although they are only for in the principal plane.

1.2 Hansen 1977

Uses spherical crater sections and normalizes wavelength to $\lambda_{max} = 2900\ \mu\text{m}^\circ\text{K}\ /0.905T_{max}$ where the .905 is empirical based on earlier thermal observations of asteriods.

Fig 6 has his beaming functions. His appendix contains the crater model, which is solved numerically.

1.3 Hapke 1984

p43.4a <<>> (4) It is assumed that the surface is made up of facets tilted at a variety of angles which have no preferred direction in azimuth but can be described by a Gaussian distribution in zenith angle. <<>>

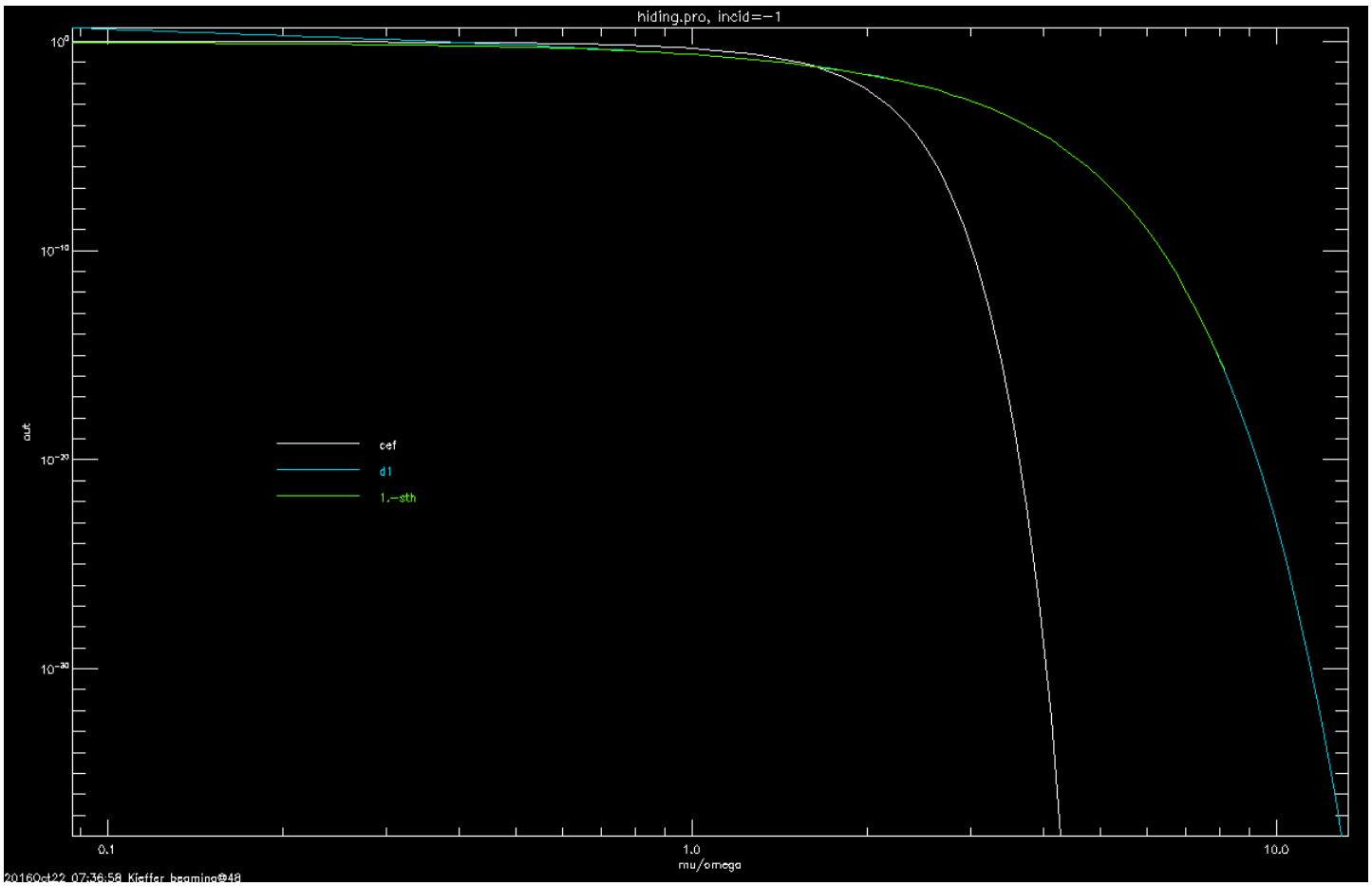

Figure 2: Terms within the basic shadow hiding function. cef (white) is the erfc $\left(\mu/\sqrt{2}w\right)$; d1 (blue) is $\frac{1}{2}\sqrt{2/\pi}\cdot\frac{w}{\mu}e^{-(\mu^2/2w^2)}$, the first term in the denominator and is >1 for $x\equiv\mu/w<0.37$; 1.-sth (green) is 1-$S(\theta)$. hidp.png

p43.0b <>> No other assumptions about the geometry of the roughness are made. The present treatment attempts to keep the morphology as general as possible.

The general procedure of the derivation will be as follows. First, expressions which are mathematically rigorous will be derived and the parameters necessary for their evaluation defined. Since the effects are maximum at grazing illumination and viewing, these expressions will be evaluated exactly under these conditions. To obtain useful approximations the equations will also be evaluated for vertical viewing and illumination. The resulting expressions will be connected by analytic extrapolation to give a solution for intermediate angles. <<>

p43.6b <>> The normals to the facets are tilted at various angles θ with respect to the local vertical ... Let $a(\theta)$ be the function which describes the distribution of tilts. ... Let the slope distribution function be normalized so that

$$\int_0^{\pi/2} a(\theta)\ d\theta\ =\ 1 \qquad (4)$$

and characterized a mean slope angle $\overline{\theta}$ defined by

$$\tan\overline{\theta} = (2/\pi)\int_0^{\pi/2} \tan\vartheta\ a(\vartheta)\ d\vartheta \qquad (5, 12.5) \qquad <<>$$

Where two equation numbers are given, the first is for Hapke84=[3] and the second for Hapke93=[4].

p50.3: <>> Define the average value of any function $F(\theta)$ as $\langle F(\theta)\rangle = \int_0^{\pi/2} F(\theta)a(\theta)d\theta$. <<>

p50.9a <>> Since (43) contains only averages of trigonometric functions weighted by $a(\theta)$ the equations are insensitive to the exact form of $a(\theta)$ used. Two distribution functions, Gaussian and exponential, which have been widely used in planetary applications (Saunders, 1967; Hagfors, 1968) were investigated. The numerical differences between the two turned out to be quite minor; hence, the Gaussian was chosen. <<>

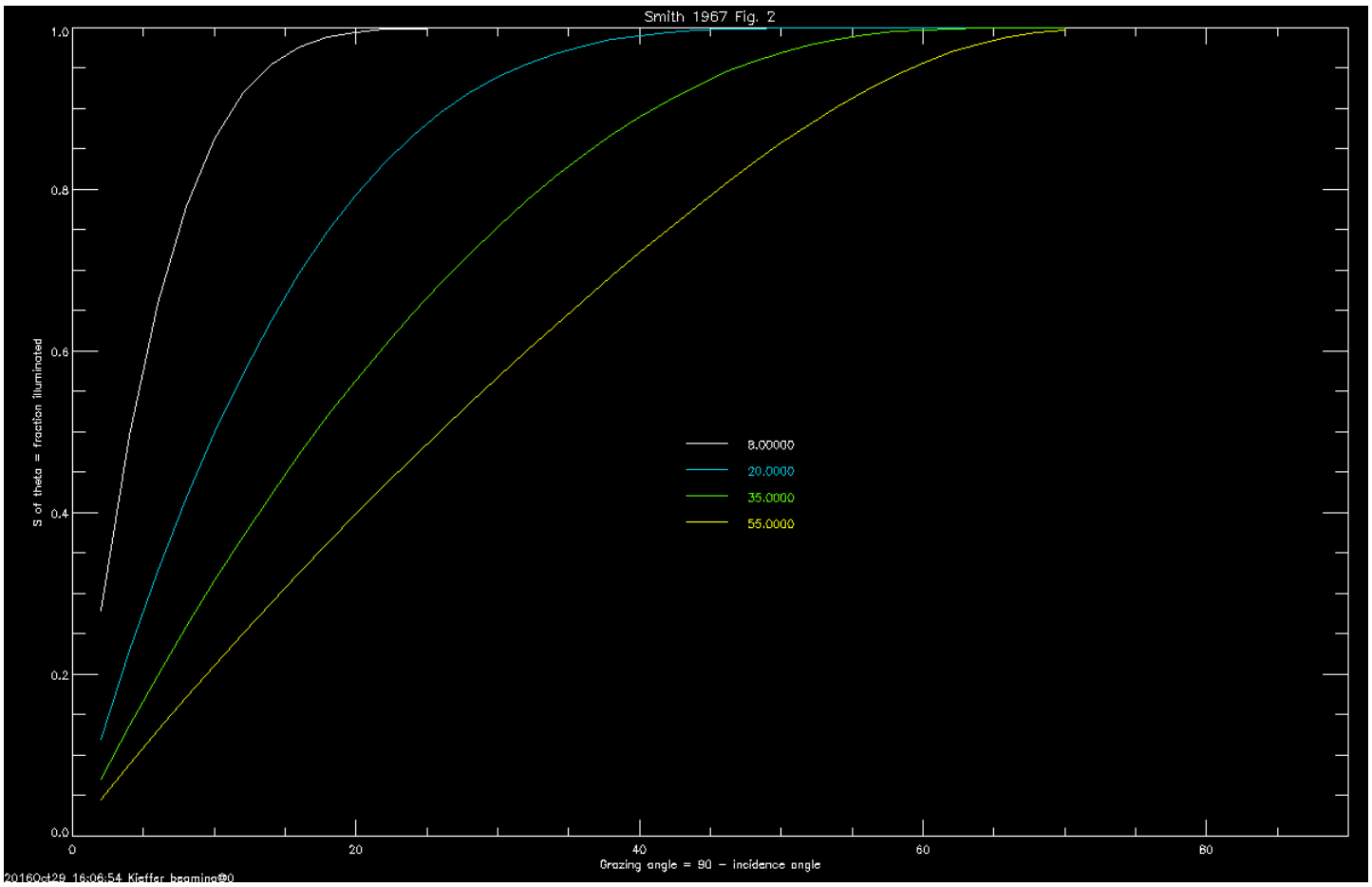

Figure 3: Reproduction of the theory part of Smith67=[8] Fig. 2. Abscissa is the "grazing angle", or 90° minus the incidence angle; the ordinate is the fraction of the surface that is illuminated. Curves are for specific RMS slope of roughness; see legend. SmithFig2.png

p51.5a: ... the distribution of slopes on any vertical cut with arbitrary azimuth through the surface <>> is assumed to be of the form $a_1(\theta)\ d\theta = A \exp\left[-\tan^2\theta / B\tan^2\overline{\theta}\right]\ d\,(\tan\theta)$, where A and B are constants. In general, if $a_1(\theta)\ d\theta$ is the one-dimensional distribution, then the corresponding two-dimensional, azimuth-independent slope distribution function is $a_1(\theta)\sin\theta d\theta d\zeta$ (Hagfors, 1968). Thus $a(\theta)$ is taken as

$$a(\theta) = A \exp\left[-\tan^2\theta\ /\ B\tan^2\overline{\theta}\right] \sec^2\theta \sin\theta. \qquad (44)$$

Assumption (2), that the mean slope $\overline{\theta}$ is not too large, will now be used for the first time. ... it is found that to second order in $\overline{\theta}$,

$A = 2/\pi \tan^2\overline{\theta}$

$B = \pi$ <<>>

And he proceeds to use approximations to second order in $\overline{\theta}$. For the remainder of Hapke roughness development I use his book as the formulation is clearer.

1.4 Jakosky 1990

Jakosky90=[5] Measures brightness temperatures of natural and artificial surfaces at several angles near simultaneously. Rougher surfaces showed the strongest incidence and azimuth angle effects.

1.5 Hapke 1993

Hapke93=[4] is a book compiling his work on scattering.

Distinguishes "tilt shadow", when a surface normal is more than 90° from the illumination or observation direction, from "projected shadow" when another part of the surface obstructs the ray. KRC 3.4 fully accounts for tilt-shadow but does not treat projected shadow.

Hapke93=[4] chapter 12 is mild rewrite of Hapke84=[3].

p326.6 <>> Then, in general (Hagfors, 1968) if $a'(\vartheta)$ is the one-dimensional function that describes the distribution of slopes on any vertical cut through the surface made at an arbitrary azimuth angle, the corresponding two-dimensional, azimuth-independent distribution function can be written in the form

$$a(\vartheta)\ d\vartheta\ d\zeta = a'(\vartheta)\sin\vartheta\ d\vartheta\ d\zeta. \qquad (12.1)$$

It will be assumed that $a'(\vartheta)$ can be described by a Gaussian distribution of the form

$$a'(\vartheta)\ d\vartheta = \mathcal{A}\exp\left[-\mathcal{B}\tan^2\vartheta\right]\ d(\tan\vartheta), \qquad (12.2)$$

where $\mathcal{A}$ and $\mathcal{B}$ are constants to be determined. Then

$$a(\vartheta) = \mathcal{A}\exp\left[-\mathcal{B}\tan^2\vartheta\right]\sec^2\vartheta\sin\vartheta \qquad (12.3)\ \text{<<>}$$

Normalizing so that the total distribution over $0{:}\pi/2$ is unity, he finds

$$\mathcal{A} = 2/\pi\tan^2\overline{\theta} \qquad \text{and} \qquad \mathcal{B} = 1/\pi\tan^2\overline{\theta} \qquad (12.6a,b)$$

Using (12.6) yields the same relation as in Hapke84=[3] near Eq. 44.; a relation similar to that shown in Shepard95=[7] Eq. 13 and Bandfield15=[2] Eq. 1; the latter is repeated reformed here for convenience

$$P(\theta) = \frac{\tan\theta}{\tan^2\theta_0}\exp\left[-\frac{\tan^2\theta}{2\tan^2\theta_0}\right]$$

Note: substitution of (12.6) into (12.3), yields

$$a(\theta) = \frac{2}{\pi}\cdot\frac{1}{\tan^2\overline{\theta}}\exp\left[-\frac{\tan^2\vartheta}{\pi\tan^2\overline{\theta}}\right]\cdot\sec^2\theta\sin\theta \qquad (1)$$

identical to 1984 work with substitution of A and B into (44). Substituting this result into (12.5), I get

$$\tan\overline{\theta} = \frac{2}{\pi}\int_0^{\pi/2}\underbrace{\frac{2}{\pi}\cdot\frac{\tan\vartheta}{\tan^2\overline{\theta}}\exp\left[-\frac{\overbrace{\tan^2\vartheta}^{Z}}{\pi\tan^2\overline{\theta}}\right]}_{\sim P(\theta)}\sin\theta\cdot\underbrace{\sec^2\theta\ d\vartheta}_{d\ \tan\theta} \qquad \text{eq : mytb} \qquad (2)$$

This has the same form but different constants, including in the exponent, as the above two citations. It produces a normalized distribution distinct from them because of the π rather than 2 in the exponent. Z is a term that differs between Hapke93=[4] and Bandfield15=[2] and which must be constrained to avoid underflow.

P 331.8 <>> ... we will try to write the rough-surface bidirectional reflectance $r_R(i,e,g)$ as the product of a shadowing function $S(i,e,g)$ and the bidirectional reflectance $r(i_e,e_e,g)$ of a smooth surface of effective area A_e tilted so as to have effective angle of incidence i_e and angle of emergence e_e, and with the same phase angle g. That is, we will seek expressions for $i_e(i,e,g)$, $e_e(i,e,g)$, and $S(i,e,g)$ that will make the following equation true:

$$r_R(i,e,g) = r(i_e,e_e,g)S(i,e,g) \qquad (10,12.10)\ \text{<<>}$$

In chapter 12, Photometric effects of large-scale roughness, at the start of his derivation, Hapke93=[4] states: p 333.7
<>> We shall follow Sanders (1967) and assume that any facet that is not in a tilt shadow has a statistical probability of being in a projected shadow that is independent of the slope or azimuth of its tilt. <<>

Eq. (12.29): relative azimuth dependence $f(\Psi) = \exp\left(-2\tan\frac{\Psi}{2}\right)$, which is a pragmatic function that <>> decreases linearly from a value $f(0) = 1$ to $f(1) = 1 - \frac{2}{3} = \frac{1}{3}$ and then decreases to zero as $\Psi \to \pi$ <<> .

Finds solutions for two conditions: first **when i $\leq$ e**

$$S(i,e,\psi) = \frac{\mu_e}{\mu_e(0)}\frac{\mu_0}{\mu_{0e}(0)}\frac{\chi(\overline{\theta})}{1-f(\psi)+f(\psi)\chi(\overline{\theta})Z} \tag{12.50}$$

where my Z is his $[\mu_0/\mu_{0e}(0)]$

$$f(\psi) = \exp(-2\tan\frac{\psi}{2}) \tag{12.51}$$

$$\chi(\overline{\theta}) = \langle\cos\vartheta\rangle = 1/\sqrt{1+\pi\tan^2\overline{\theta}} \tag{12.45a}$$

obtained by assuming ($\overline{\theta}$ is small and expanding to second order, as discussed before Eq (12.41a)

$$E_1(x) = \exp\left(-\frac{2}{\pi}\cot\overline{\theta}\cot x\right) \tag{12.45b}$$

$$E_2(x) = \exp\left(-\frac{1}{\pi}\cot^2\overline{\theta}\cot^2 x\right) \tag{12.45c}$$

$$\mu_{0e}(\psi) = \chi(\overline{\theta})\left[\cos i + \sin i\tan\overline{\theta}\,\overbrace{\frac{\cos\psi E_2(e)+\sin^2(\psi/2)E_2(i)}{2-E_1(e)-(\psi/\pi)E_1(i)}}^{r46}\right] \tag{46, 12.46}$$

$$\mu_e(\psi) = \chi(\overline{\theta})\left[\cos e + \sin e\tan\overline{\theta}\,\overbrace{\frac{E_2(e)-\sin^2(\psi/2)E_2(i)}{2-E_1(e)-(\psi/\pi)E_1(i)}}^{r47}\right] \tag{47, 12.47}$$

In the above two equations I have added the (ψ) to the left side for clarity

$$\mu_{0e}(0) = \chi(\overline{\theta})\left[\cos i + \sin i\tan\overline{\theta}\frac{E_2(e)}{2-E_1(e)}\right] \tag{48, 12.49}$$

$$\mu_e(0) = \chi(\overline{\theta})\left[\cos e + \sin e\tan\overline{\theta}\frac{E_2(e)}{2-E_1(e)}\right] \tag{49, 12.48}$$

When e $\leq$ i:

- (12.46) is modified by replacing the term r46 with r47 and exchanging $i \Leftrightarrow e$ therein to make (12.52)
- (12.47) is modified by replacing the term r47 with r46 and exchanging $i \Leftrightarrow e$ therein to make (12.53)
- my Z in (12.50) becomes $[\mu/\mu_e(0)]$ to make (12.54)

These equations were implemented in **hapkes.pro**; results covering a wide range of i,e, and ψ are shown in Figures 4 and 5. The function generally decreases with increaseing incidence angle and the variation alnog azimuth increases with increaseing emergence angle.

The increase toward large azimuths for high emergence angles seems non-physical.

The azimuth function is shown in Fig. 6

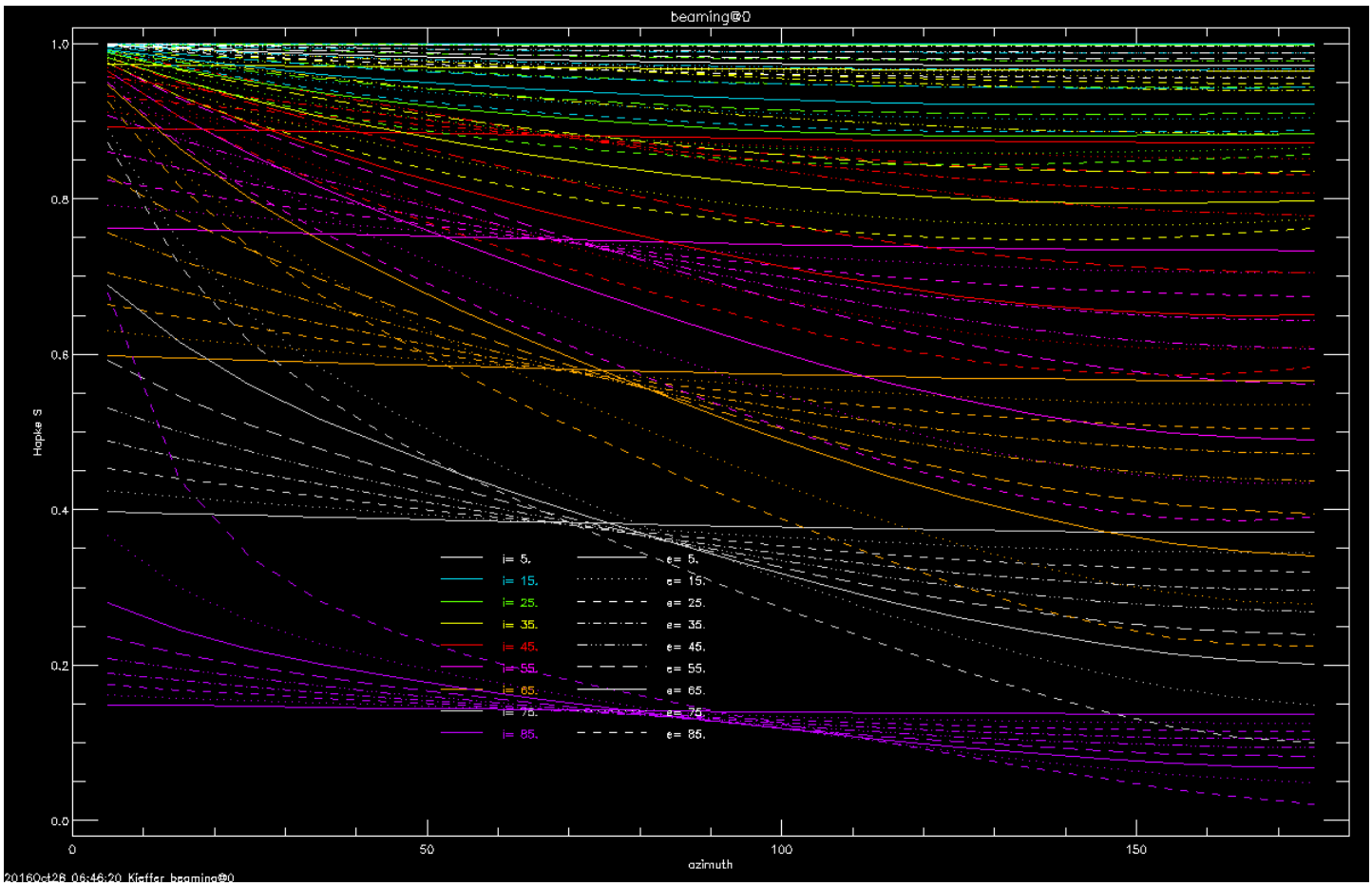

Figure 4: Hapke shadow function for incidence and emergence angle of 5 to 75° and relative azimuths 5 to 175° for a roughness mean slope of 30°. Each color (see left legend) is for a single incidence angle; emergence angle is indicated by line type (see right legend) hapkes.png

1.6 Shepard 1995

Based on the concept of fractal sufaces. Fractal surface statistics based on uniform separation of points in the horizontal plane, so that a $\cos\theta$ term is not needed to in finding the mean angle or slope.

In §2.1 defines several terms: <>>

5. Variance (σ^2). The variance of all points on a surface or profile aboutn the mean value:

$$\sigma^2 = \langle [z - \overline{z}]^2 \rangle \qquad (1)$$

9. Slope histogram ($P(s) = P(\tan\theta)$) . A function describing frequency or number slopes within any angular interval. Note that s is the slope or tangent of slope angle θ) 0.

10. Slope density function or slope distribution ($p(s) = p(\tan\theta)$). A function describing frequency or number of slopes within any solid-angle interval. The slope density function is essentially the slope histogram normalized by solid angle. The difference will become apparent when unidirectional and adirectional slope distributions are discussed. <<>

In §3.3 discusses three slope distributions of fractal surfaces:

Unidirectional p11714.3 b <>> Efford [1990] notes that synthetic fractal surfaces have unidirectional slope histograms that are accurately represented by Gaussian functions. <<>

p11714.5 b <>> Therefore, the unidirectional slope distribution of a fractal surface is Gaussian, with (slope) variance $< (\Delta z/\Delta x)^2 >$. The rms slope is just the square root of this variance and is typically converted to degrees by taking the inverse tangent. <<>

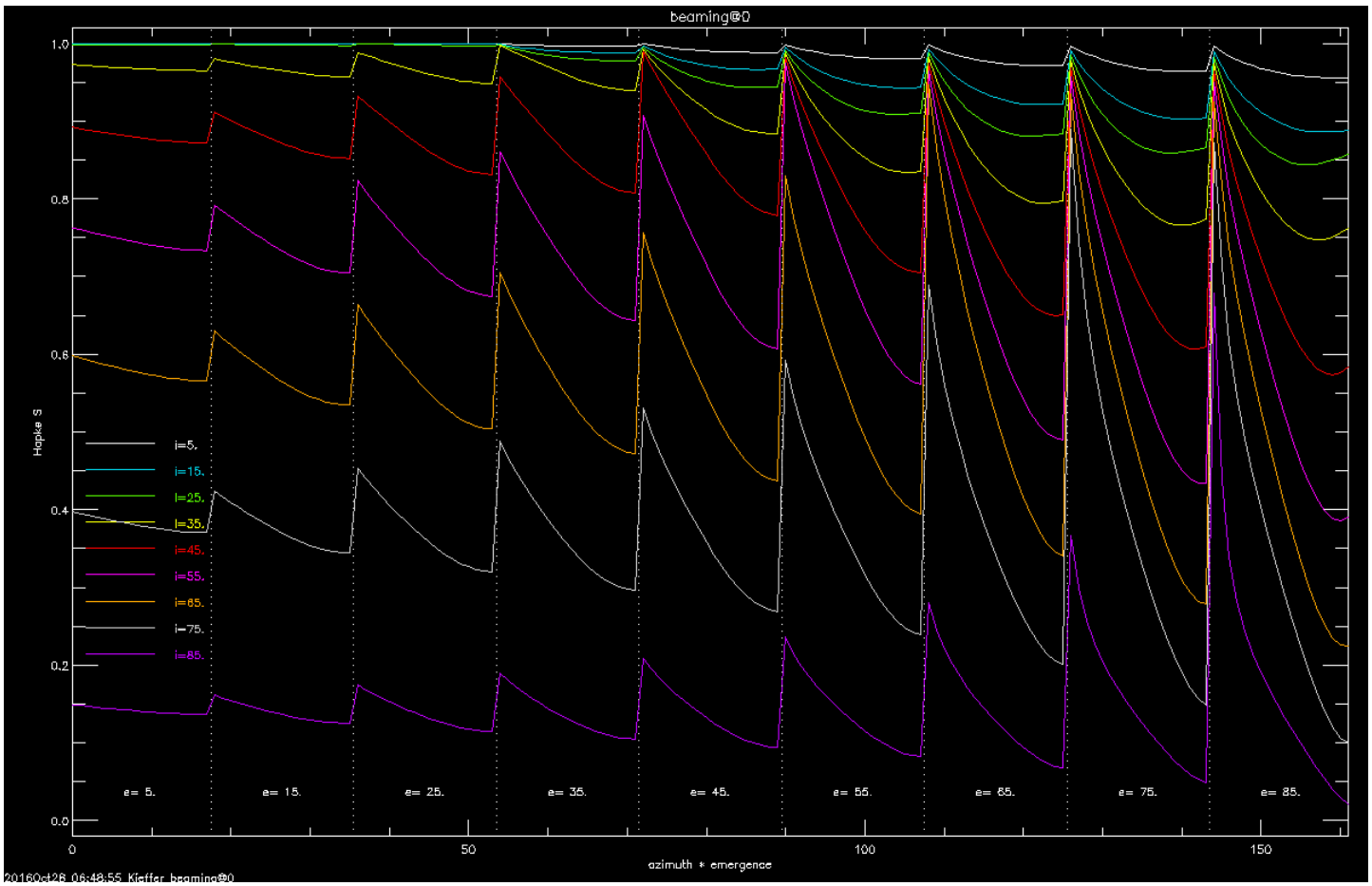

Figure 5: Hapke shadow function, see caption for Fig. 4. Each curve (see legend) is for a single incidence angle; azimuth increase radiply to the right repeatedly, each section is for an emergence angle indicated by labels near the bottom of the chart. hapkes2.png

p11714.7 b <>> Although seemingly a trivial distinction, the unidirectional slope angle distribution of a fractal surface will not be Gaussian, except in the limit as $\theta_{\rm rms} \rightarrow 0$. This is because the inverse tangent is increasingly nonlinear at higher slopes. <<>

Adirectional Closely follows a Rayleigh distribution: <>> ... defined by

$$P(s) = \frac{s}{s_0^2} e^{-(s^2/2s_0^2)} \qquad (13)$$

where P is the slope histogram function, s is the slope of the surface normal polar angle, and s_o is the mode of the distribution, equal to the unidirectional rms slope. <<>

Effective <>> We define the effective surface slope following Campbell and Garvin [1993] as:

$$s_{\rm EFF} = \frac{\sqrt{2}\sigma}{l} \qquad (18)$$

where l ... is the autocorrelation length <<>

Refers to: Simpson, A., and G. L. Tyler, Radar scattering laws for the lunar surface. IEEE Trans. Antennas Propagat., AP-30, 438-448, 1982

1.7 Bandfield 2008

§2.4, ¶2 <>> We chose to use the θ -bar parameter described by Hapke (1984) as a model for surface slopes (Fig. 2). This model is based on a Gaussian distribution of slopes along a surface cross-section that is expanded to a full three dimensional

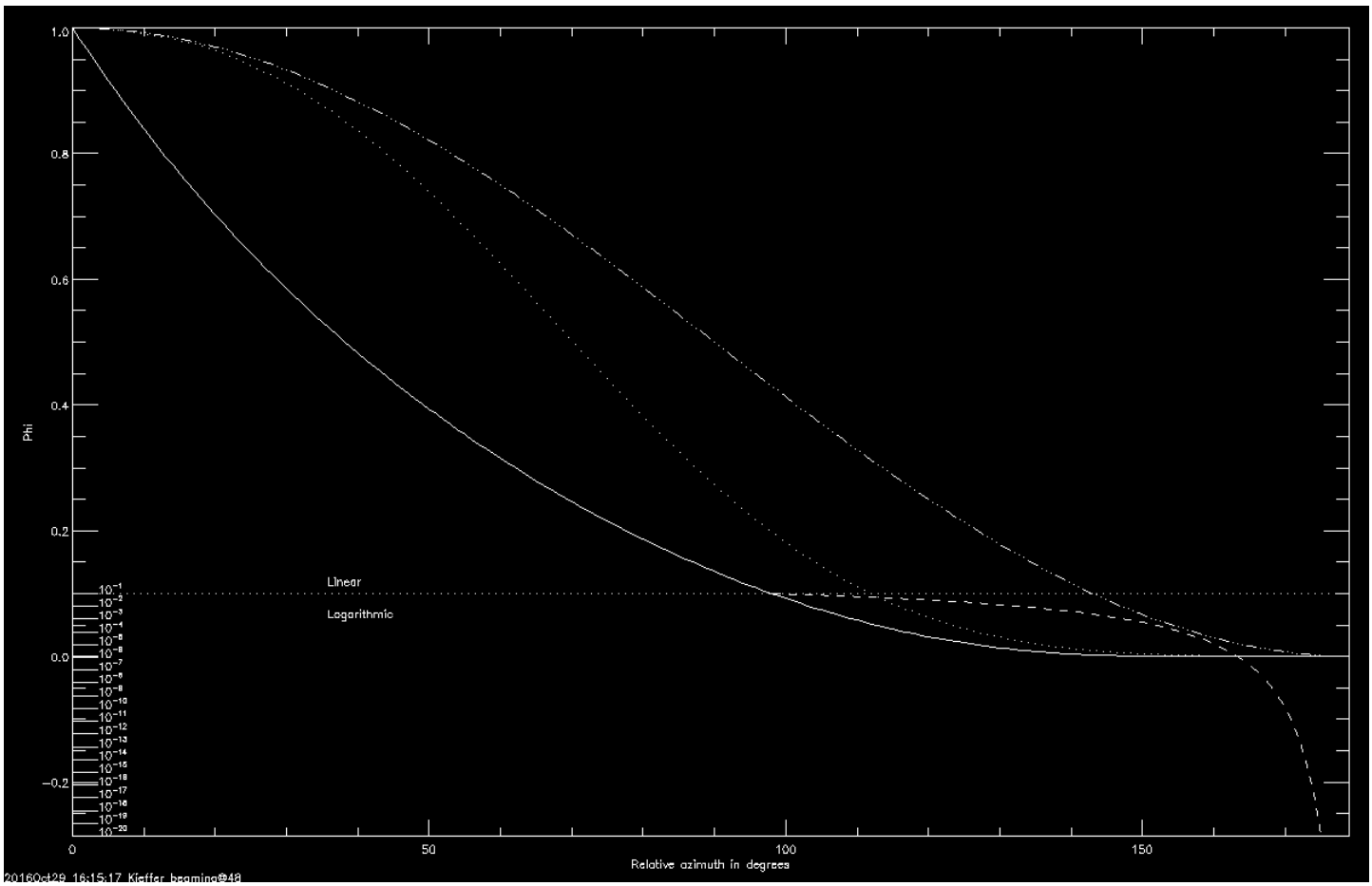

Figure 6: The azimuth function $f(\Psi)$ of Hapke93=[4], Eq. (12.29). Below 0.1, the solid line shows the approach to 0 in the forward scatter direction on a linear scale and the dashed line on a logrithmic scale (20 orders of magnitude; scale at the left margin. The $-\cdots$ line shows the simplistic function with continuous derivatives $\frac{1+\cos\psi}{2}$ and the dotted line is a compromise function $\frac{1+\cos(\psi(1+.3\sin\psi))}{2}$ closer to $f(\Psi)$. hida.png

surface assuming that the azimuths of slopes are random. This model is independent of length scales and can be described using a single parameter. While this simplicity is well suited for the derivation of surface slope distributions from the data, it is not adequate for geological interpretation of surfaces as it does not account for the scale at which the roughness occurs. ≪◇

1.8 Bandfield 2015

Bandfield15=[2] uses the relations of Smith67=[8] for shadowing at nadir view. The relative azimuth dependence for off-nadir illumination and viewing comes from Hapke84=[3].

p 358.9b: §2.1
◇≫ Our thermal model assumes radiative equilibrium to predict surface temperatures. Sloped surfaces include a downwelling radiative component proportional to the fraction of the hemisphere filled by adjacent surfaces rather than space. To maintain computational efficiency, the solar and thermal infrared downwelling radiance is calculated assuming it is coming from a horizontal surface at radiative equilibrium. ≪◇

p 359.4a §2.2. Surface roughness model
◇≫ We use a simple Gaussian roughness model that is similar to that described by Helfenstein and Shepard (1999) and has been used for comparison to martian TIR datasets (Bandfield and Edwards, 2008; Bandfield, 2009). Surface temperatures are predicted for slopes of 090° at 2° intervals and azimuth orientations of 0360° at 20° intervals. The radiance of each slope/azimuth combination is calculated, and its contribution to the total modeled radiance is weighted by the statistical probability of its occurrence. This reduces the surface slopes/roughness to a single parameter (RMS slope) that is independent of length scales while maintaining reasonable fidelity to natural surfaces.

The probability distribution P for a given slope angle, θ, is described by the following (derived from Eq. (13) of Shepard et al. (1995)):

$$P(\theta) = \frac{\tan\theta}{\tan^2\theta_0} \cdot e^{-\frac{\tan^2\theta}{2\tan^2\theta_0}} \qquad (1)$$

where θ_0 is the tangent of the RMS slope angle. This describes the adirectional distribution of slopes, which closely approximates a Gaussian distribution of unidirectional slopes for a RMS slope angle of θ_0 (Shepard et al., 1995). For our purpose, the azimuth direction for the slope of any given surface has no preferential orientation and our measurements are sensitive to an adirectional distribution of slopes with random azimuths rather than the slope distribution along any particular transect or orientation. <<>

The above statement " θ_0 is the tangent of the RMS slope angle" seems to be in error as his Eq. 1 would then be taking the tangent of a tangent.

p 359.9a
<>> We use a shadowing approximation methodology modified from that developed by Smith (1967) and Hapke (1984) . This model assumes that any slope/azimuth surface that would otherwise be illuminated has the same statistical chance of being within a shadow cast by another surface. This is a relatively simple approach for nadir observations described by the following (derived from Eqs. (21) and (24) of Smith (1967)):

$$S(\theta) = \frac{1 - \frac{1}{2}\mathrm{erfc}\left(\mu/\sqrt{2}\omega\right)}{\frac{1}{2}\left(\sqrt{2/\pi} \cdot \frac{\omega}{\mu} e^{-(\mu^2/2\omega^2)} - \mathrm{erfc}\left(\mu/\sqrt{2}\omega\right)\right) + 1} \qquad (2)$$

where $S(\theta)$ is the fraction of the shadowed surface, μ is the cotangent of the solar incidence angle, ω is the RMS surface slope distribution, and erfc(x) is the complementary error function (the integral between 0 and x of a Gaussian distribution function).

This equation can only be applied as is to nadir observations where no surface is hidden from the spacecraft view (assuming no overhanging surfaces). <<>

p 359.4b
To account for viewing orientation effects, we use an approach similar to that described by Hapke (1984). Where the viewing emission angle is greater than the solar incidence angle, the shaded fraction observed at nadir, $S_{nadir}(\theta)$, is modified by the following:

$$S_{view}(\theta) = S_{nadir} \cdot \left(1 - e^{-2\tan\left[\frac{1}{2}(\phi_{sun} - \phi_{obs})\right]}\right), \qquad (3)$$

where $S_{view}(\theta)$ is the fraction of shadowing that is present within the field of view, ϕ_{sun} is the azimuth angle of the Sun with respect to the surface, and ϕ_{obs} is the azimuth angle of the spacecraft with respect to the surface. Where the viewing emission angle is less than the solar incidence angle, the following applies:

$$S_{view}(\theta) = S_{nadir} - S_{obs} \cdot e^{-2\tan\left[\frac{1}{2}(\phi_{sun} - \phi_{obs})\right]} \qquad (4)$$

where S_{obs}) is the shadowing function described in Eq. (1) , except as applied to the viewing incidence angle of the spacecraft rather than the Sun. <<>

§3.2.3, p360.6b
<>> Modeling indicates that surface roughness has little effect where solar incidence is less than $\sim 30°$, and these observations can be considered free of its interfering effects (Davidsson et al., submitted for publication) <<>

Fig 6 has some effects of slopes of 10,15,20,15 °.

§4.2.1. Day, p 363.9a
<>> The six daytime EPF observations acquired with moderate angles of solar incidence (Table 2 and Fig. 7) all show a distinct asymmetry in brightness temperature about the nadir observation. In each case, the measurement pointing equatorward has lower brightness temperatures than the equivalent emission angle observation that points poleward. <<>

p 363.4b
<>> As expected, both the model and Diviner measurements show a trend of increasing temperature differences at higher opposing emission angles. Temperature differences reach ~ 63 K for the EPF observation near 98°E, 52°S at opposing 7° up- and down-track emission angle observations. The modeled temperature differences also predict increasing temperature differences for higher RMS surface slope distributions. The six daytime EPF sequences compare most closely with modeled surface slope distributions of $\sim 25 - 35$ °(Fig. 9). <<>

2 Outline of pragmatic formulations

Divided into two major sections

Distribution of slopes; i.e. the physical surface independant of its temperature

Temperatures of the seen surface, and effect upon that of the far field it sees

Distributions should cover the complete range of physical likelyhood. E.g. dips (slope relative to horizontal) from 0 to 90°, will ignore overhangs; all azimuths, both abolute (e.g., from North) and relative (from the plane of incidence). Functions must be continuous, and it is desireable that at least the first dervative be continuous. Yet, the presence of "ponded deposits" of zero slope would require a discontinuous first derivative in slope abundance

2.1 Devils enumeration of approximations

UniAlb Material albedo is the same for all slopes. Unknown.

UniPhot Material reflectance function is the same for all slopes. Unknown.

UniLay Material subsurface properties are the same for all slopes. Unlikely but magnitude unknown.

SlopeElev Slope probablility is not related to elevation. Depends upon geology.

ffT Far-field temperature is the same at all azimuths. Poor; address.

ShadeTilt Temperature in the shade independent of tilt. Poor; address.

ShadeTime Temperature in the shade independent of hour. Poor.

EmissLamb Thermal emission of a facet is Lambertian. Reasonable, accept.

AbsAzi Absolute azimuth does not matter. Thought to be excellent.

KofT Conductivity not a function of temperature. Addressed by KRC.

Homog Material is homogeneous with depth. Addressed by KRC.

Sphere Object is spherical. Knowable and addressable; harder if concave.

Geography Object is the same at all locations (lat/long) / / OK initially. Addressable by mapping models.

2.2 Distribution of elevations and slopes

I generate the IDL routine **hiding.pro** to compute shadow and hiding functions; negative incidence angles generate various plots.

[concave / convex] As a multiplier of the theoretical distribution

2.3 RMS slope of a sphere

Using Hapke84=[3] definition of mean slope angle (his Eq. 5), the mean slope of the visible half of a sphere (or a hemispherical crater) is

$$\overline{\theta} \equiv \int_0^{\pi/2} \tan\theta \cdot \sin\theta \ \cos\theta \ d\theta \Rightarrow \int_0^{\pi/2} \sin^2\theta \ d\theta \Rightarrow \left[\frac{\cos^3\theta}{3} - \cos\theta = \frac{2}{3} \right]_0^{\pi/2} \qquad \text{and} \qquad \theta = 33.7^\circ \tag{3}$$

2.4 Probability of hiding

2.5 Aside on Hiding

A hiding function can be used on the incidence angle i to calculate the likelyhood that a tile segment in shadow; but existing functions say nothing about how long has it been in shadow. A hiding function can be used on the emergence angle e to calculate the population of tilt facets that the viewer sees. The hiding function should be symmetric with respect to i and e.

In the morning, a facet it has probably been in shadow through the prior night, so using the pre-dawn temperature would be appropriate. In the afternoon, would need to estimate when that tilt might have entered shadow; this would require integrating the probability that it was in shadow from noon to the current time.

2.5.1 Implication of geology

Hapke shadowing formalism is used by several authors. I have a problem with the p333.7 assumption as my experience is that in rugged terrain steeper slopes have a lower probability of being shadowed; this is partially because steep slopes are commonly higher in the terrain where there is less terrain above them to generate debris that would bury them to make shallower slopes! This results when surface degradation rates are relatively uniform over area, as for example by thermal fracturing.

One inportant exception on Earth includes "hill and valley" terrain, where erosion is dominated by rainfall and fluid flow, a strongly non-linear process, and surfaces become convex upward apart from the negative cusp of the stream/river itself.

Since this is an effect of gravity, it might be less important on asteroids; but the modest set of high-resolution images from small bodies (e.g., the Rosetta mission, 433 Eros imaging by NEAR) suggest that gravity has some effect on them as well. Diurnal thermal cycling will tend to disaggregate blocks larger than a modest fraction of the diurnal skin depoth. Disaggregation and motion due to seismic waves from impacts is discussed by Richardson05=[6].

This leads me to wonder if a "hiding" function weighting visibility as a function of facet slope would be appropriate.

For dark objects, where multiple scattering is unimportant, visibility increasing with slope would lead to limb brightening relative to a Lambertian sphere.

2.5.2 Discussion

If radiative equilibrium is assumed, then all solar shadows are at 0K; modelers usually assume some realistic fixed value, Bandfield15=[2] uses 100K.

To improve on this would require treating what tilt is in the shadow and how long it had been is shadow.

A limiting realistic case is to set the temperature of a tilt that is in shadow to the minimum diurnal temperature for that site and conditions. This is not impractical with the KRC formalism used here.

2.6 Distribution of tilt within visibility

Visibility V is here defined as simply 1.-hiding, or $V \equiv 1 - H$

Allow a modification of hiding related to tilt under the requirement that the total hiding or visibility does not change.

H=$H_0 F(x)$ where x is the dip angle of a facet, and require $\int_0^{\pi/2} F(x)p(x) = 1$ where $p(x)$ is the population function of dips and $\int_0^{\pi/2} p(x) = 1$.

A simple implemenation is F as a Chebyshev polynomial of the first kind in $x = 2p/p_{\max} - 1$; i.e., $Y = c_0 + c_1 x + c2(2x^2 - 1) + ...$, $F = Y/\int_0^{\pi/2} Y(x)p(x)\ dx$ and degree 2 should be enough. Without loss of generality, can let $c_0 = 1$ and this will be convenient. F must not be negative anywhere.

2.7 Effect of azimuth

The azimuth function derived by Hapke93=[4], Fig. 6, has a discontinuous slope crossing the backscatter plane; which might be physical only for zero phase angle. A simplistic function that as continuous derivatives and the same limits as his Eq (12.51) is $\frac{1+\cos\psi}{2}$.

To account for the tendency of a slope in rough terrain to be facing slopes of the opposite azimuth, e.g., a west-facing slope near dusk is likely to view warm east-facing slopes in the far field, generate KRC models wherein each tilt facet uses a far-field with a tilt near the RMS slope value and an azimuth different by 180°.

2.8 Nature of the far field

None The far field (below the horizon) has zero radiance. This is non-physical but is simple to do and has been done in some asteroid papers to estimate the magnitude of the far-field effect. KRC has not had this capability, but version 3.4 could

emulate it by using a far-field file with a negligable temperature.

Self The far field is the same temperature as the tilted surface. This was done in KRC before version 3

Flat The far field has the temperature of a flat (zero dip) surface of the same material. KRC 3+ has the option for the far field surface temperature to be that of any prior run, and normally this would be a run with identical materials with zero slope.

Opposite Assign the far field the temperature of the RMS slope at same time of day but 180° difference in azimuth from the subject facet. This could be closely approximated by running a set of KRC models first flat, then with the RMS slope using flat as the far field at all azimuths, then a full set of tilts with each azimuth using the opposite-azimuth RMS slope model as the far-field file.

3 numerical results

Slope distributions were calculated several ways, using slope angles every 0.1° from 0.1 to 89.9. For each distribution, the terms were separated into elements variable with angle, whose product is F_i and all those constant with angle. The

$d\tan\theta$ was implimented both numerical based on mid-point between each angle θ and $\sec^2\theta d\theta$; the two differ by less than one ppt below 88.3°/

Hapke Equation Eq. 2. Constant= $(2.\cdot 2.)/(\pi\cdot\pi\cdot$ *d. tan*θ numerical based on mid-point between each angle θ

Bandfield Similar to Equation Eq. 2 except the π in exponent section replaced with a 2. All else the same as above, His θ_0 is taken to be the RMS slope angle

literal Similar to Bandfield version, except Bandfield θ_0 is taken literally to be tangent of the tangent of the RMS slope angle.

3.0.1 Averaging

In each case, first compute a distribution that totals to unity over the set of uniform angles used. All except "Hapke" below use this distribution F

Hapke As shown in Eq. Eq. 2, then convert to angle and to degrees

MnAng Mean angle: $m = \sum_{i=1}^{N} p_i F_i$

RMSan $r = \sqrt{\sum_{i=1}^{N} p_i^2 F_i^2}$

RMSsl

RMStd

7

References

[1] J. L. Bandfield and C. S. Edwards. Derivation of martian surface slope characteristics from directional thermal infrared radiometry. *Icarus*, 193:139–157, January 2008.

[2] J. L. Bandfield, P. O. Hayne, J.-P. Williams, B. T. Greenhagen, and D. A. Paige. Lunar surface roughness derived from LRO Diviner Radiometer observations. *Icarus*, 248:357–372, March 2015.

[3] B. W. Hapke. Bidirectional reflectance spectroscopy, 3. correction for macroscopic roughness. *Icarus*, 59:41–59, 1984.

[4] B. W. Hapke. *Theory of Reflectance and Emittance Spectroscopy.* Cambridge University Press, Cambridge, 1993. 455 pp.

[5] B. M. Jakosky and R. M. Haberle. Year-to-year instability of the Mars south polar cap. *J. Geophys. Res.*, 95:1359–1365, 1990.

Table 1: Mean roughness for three distribtions averaged five ways. See text for explanations

i	Theta-bar in	1.000	2.000	5.000	10.000	15.000	20.000	25.000	30.000
0	Hapke:Hapke	0.999	1.994	4.914	9.385	13.211	16.400	19.043	21.247
1	Hapke:MnAng	1.998	3.988	9.817	18.732	26.436	33.030	38.730	43.743
2	Hapke:RMSan	2.169	4.326	10.617	20.093	28.103	34.827	40.548	45.517
3	Hapke:RMSsl	2.169	4.331	10.694	20.573	29.270	36.791	43.288	48.941
4	Hapke:RMStd	2.504	4.992	12.214	22.930	31.782	39.051	45.115	50.286
5	2angl:Hapke	0.508	1.014	2.516	4.904	7.086	9.037	10.769	12.306
6	2angl:MnAng	1.595	3.186	7.891	15.322	22.065	28.104	33.526	38.446
7	2angl:RMSan	1.731	3.456	8.544	16.493	23.579	29.815	35.328	40.265
8	2angl:RMSsl	1.731	3.459	8.586	16.770	24.318	31.168	37.358	42.964
9	2angl:RMStd	1.999	3.990	9.843	18.888	26.807	33.646	39.587	44.817
10	2slop:Hapke	0.507	1.011	2.461	4.517	5.991	6.908	7.370	7.485
11	2slop:MnAng	1.595	3.182	7.835	14.950	21.083	26.308	30.805	34.746
12	2slop:RMSan	1.731	3.452	8.484	16.103	22.573	28.014	32.647	36.674
13	2slop:RMSsl	1.731	3.455	8.524	16.363	23.243	29.217	34.446	39.098
14	2slop:RMStd	1.998	3.985	9.774	18.457	25.737	31.798	36.925	41.364

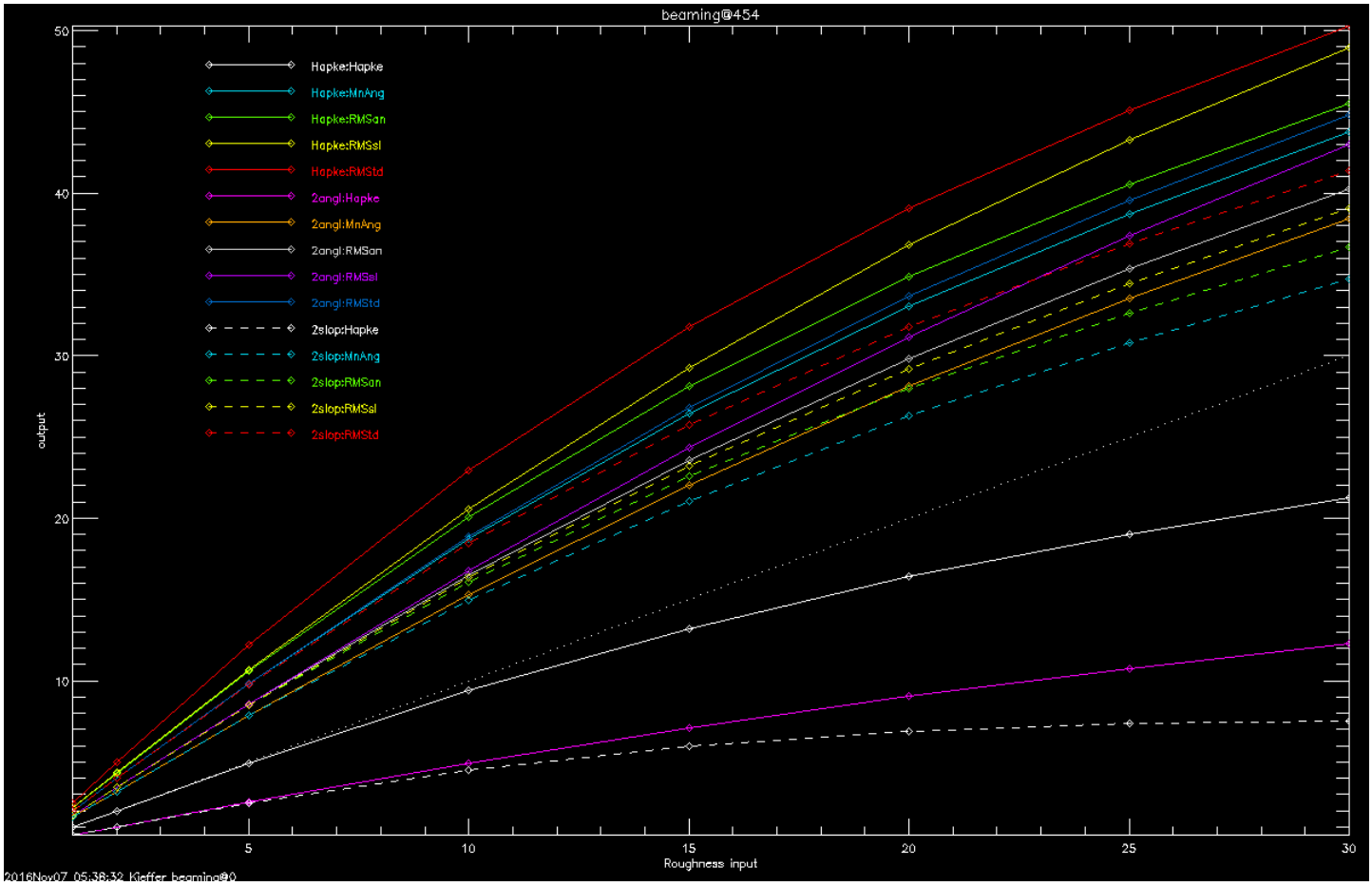

Figure 7: Mean angle of roughness for three kinds of slope distributions and 5 measures of the mean. data from Table 1 rough.png

[6] J. E. Richardson, H. J. Melosh, R. J. Greenberg, and D. P. O'Brien. The global effects of impact-induced seismic activity on fractured asteroid surface morphology. *Icarus*, 179:325–349, December 2005.

[7] M. K. Shepard, R. A. Brackett, and R. E. Arvidson. Self-affine (fractal) topography: Surface parameterization and radar scattering. *J. Geophys. Res (planets)*, 100:11790–11718, 1995.

[8] B.G. Smith. Lunar surface roughness: Shadowing and thermal emission. *J. Geophys. Res.*, 72:4059–4067, 1967.